Trapping of Solid Particles at a Wall in a Turbulent Flow

James B. Young and Thomas J. Hanratty
Dept. of Chemical Engineering, University of Illinois, Urbana, IL 61801

Studies of the motion of a dilute suspension of 100-micron glass and stainless steel spheres in water flowing turbulently down a pipe revealed that they could be trapped in necklace formations that move slowly at a distance of less than one particle diameter from the wall. The tendency toward trapping increases with particle density and decreases with flow rate. The phenomenon is interpreted as occurring when the Saffman lift force toward the wall overcomes the ability of fluid turbulence to mix the particles. The location of the particles is dictated by a balance between the Saffman lift force and a wall-induced force associated with the displacement of fluid as a particle moves parallel to the wall.

Introduction

A recent thesis from this laboratory (Young, 1989) describes the use of optical techniques to study the motion of solid spheres in a downward flowing turbulent liquid. During these experiments it was observed that under certain flow conditions the particles are trapped close to the wall at a distance of about one particle diameter. This article describes these experiments and presents a tentative interpretation. An interesting aspect is that very dilute suspensions were involved. This means that the trapping is associated with the fluid hydrodynamics and is not related to particle-particle interactions or to the influence of the particles on the fluid turbulence.

Description of the Experiments

The experiments were carried out for the downward flow of water in a 5.08-cm pipe. One hundred-micron glass or steel spheres were injected as a slurry at the same velocity as the water through a tube that had an inside diameter of 0.051 cm. The concentration of particles in the injector was about 8,200 ppm so as to give 1 ppm in the fluid flowing in the pipe.

The glass particles used in the experiments were Class IV, No. 1217 Uni-Spheres, manufactured by the Cataphote Division of the Ferro Corporation. They have an index of refraction of 1.51 and a specific gravity of 2.42. The 316 stainless steel spheres, which have a specific gravity of 8.0, were obtained from Duke Scientific Corporation. Special techniques that involved sieving and rolling-down, inclined planes were used to separate out spherical glass particles in the range 90--106 micron. The stainless steel particles were quite spherical so that only a sieving operation was needed to separate out the 90-106-micron particles.

Results

Observations of particle necklaces

Particles were injected at the center of the pipe. Far enough downstream they spread over the whole cross-section. In this part of the pipe, both the glass and the stainless steel particles were observed to be trapped near the wall. When this happens, the particles form necklaces that are aligned in the flow direction and move slowly downstream.

Qualitative observations suggest that the necklace structures are not caused by particle-particle interactions as are the formations found away from the wall in laminar flows (Segre and Silberberg, 1962). The necklaces sometimes move very close to one another without merging. When they are close, particle spacing in the azimuthal direction can be less than the spacing in the axial direction. The velocities of individual particles in a necklace are observed to fluctuate in both the axial and azimuthal directions, without being influenced by the action of the particles downstream from them. Thus, the particles do not move toward or away from the wakes of their downstream neighbors.

When the injection rate of the particles was increased, the population of particles within each individual necklace increased. The behavior of the necklaces did not change even

when the spacing of the particles was no more than 1-2 diameters.

The spacing of these necklaces was determined in an experiment with glass spheres at $Re = 16{,}200$. The number of necklaces that simultaneously occur over a 5-cm length of pipe was determined to range from 29 to 32. This gives a spacing of 0.495 to 0.546 cm for the 5.04-cm pipe. If this spacing is normalized with the friction velocity u^* and the kinematic viscosity of the fluid ν, values of 92.9–102.5 are obtained.

This is the same as the spacing of the streaky structures observed in turbulent flows close to a wall when dye is injected from a ring source at the wall. It, therefore, appears that the necklaces result from the same turbulent structures that form these streaks.

Distance from the wall

An estimate of the distance of the trapped particles from the wall was obtained by photographing them with a videocamera positioned perpendicular to the flow direction. The videotape was examined frame by frame to determine the velocity of individual particles in the flow direction. A summary of these measurements is given in Table 1, where U_P is the average of the velocities of 50 observed particles, u^* is the friction velocity, and d_P^+ is the diameter of the particle made dimensionless with the friction velocity and the kinematic viscosity.

The distance of the particle from the wall y_P can be calculated from the measurement of the particle velocity U_P since

$$U_P = U_F + (U_P - U_F) \tag{1}$$

where $(U_P - U_F)$ is the slip velocity and U_F is a function of y_P. Because of the proximity of the wall, this slip velocity cannot be set equal to the terminal velocity U_T. Brenner (1961) and Maude (1961) have shown that the force on a sphere moving parallel to the wall is given by:

$$F_{D11} = 6C_{11}\pi\mu r_P(U_P - U_F) \tag{2}$$

$$C_{11} = \left[1 - \frac{9}{16}\frac{r_P}{y_P} + \frac{1}{8}\left(\frac{r_P}{y_P}\right)^3 - \frac{45}{256}\left(\frac{r_P}{y_P}\right)^4 + \ldots\right] \tag{3}$$

where r_P is the particle radius and y_P is the distance of the particle from the wall. The increased resistance associated with the presence of the wall has the effect of decreasing the free-fall velocity.

Equation 3 for C_{11} is plotted in Figure 1. Goldman et al. (1967) recently showed that Eq. 3 becomes invalid for very small y_P/r_P. Their calculated results are shown as the solid points in Figure 1. The solid curve, which is a composite of Eq. 3 and the calculations of Goldman et al., was used in this article to evaluate C_{11}.

Table 1. Calculation of the Distance of Trapped Glass Particles from the Pipe Wall

U_P (cm/s)	Re	u^* (cm/s)	$d_P^+ = R^+/254$	U_T^+	Calc. Eq. 4 y_P/d_P	Theory Eq. 19 y_P/d_P
1.91 ± 0.21	12,700	1.40	1.52	0.56	0.65	0.52
3.16 ± 0.38	16,200	1.72	1.88	0.46	0.80	0.53
4.25 ± 0.39	18,900	1.97	2.15	0.40	0.87	0.54
5.80 ± 0.57	22,000	2.25	2.46	0.35	0.95	0.54
7.35 ± 0.83	26,100	2.61	2.85	0.30	0.91	0.56

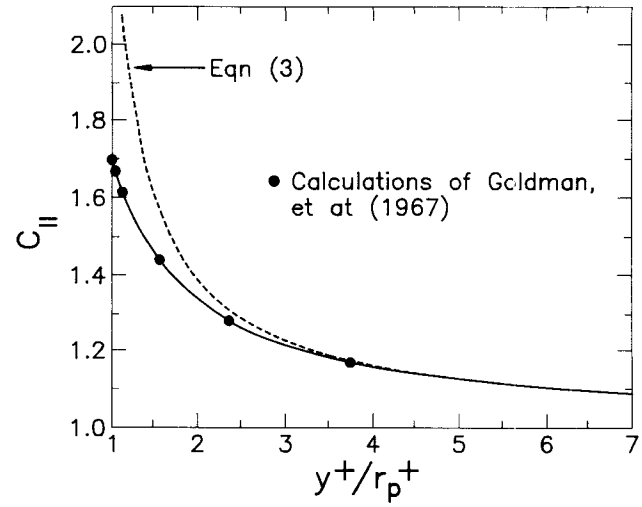

Figure 1. Correction factor for drag on particles moving parallel to the wall.

From Eqs. 1 and 2, the following equation is derived:

$$U_P^+ = y_P^+ + \frac{U_T^+}{C_{11}} \tag{4}$$

From the measurements of U_P^+ and the results for C_{11} in Figure 1, the values y_P/d_P given in Table 1 were calculated. It is noted that the average distance of the particle center from the wall increases with Reynolds number. It is of the order of unity.

Dependence on flow rate and particle density

A measure of the influence of liquid flow rate on the tendency of particles to be trapped was obtained by photographing the cross section of the pipe with a camera that viewed axially up the pipe. This was done by illuminating a 5-mm length of pipe located 392 cm from the injector.

Sample photographs for glass particles at Reynolds numbers of 16,200 and 22,000 are given in Figures 2 and 3, in which a length of the pipe wall is visible because of effects of perspective. Images of particles in the wall can be clearly seen, and the wall location is defined as the bisector of a line connecting the particle and its image. A particle is defined to be located at the pipe wall when its image is indistinguishable from its mirror image in the wall. The larger amount of trapping at the lower flow rate is indicated by a larger number of images at the wall.

Several experiments of this type were carried out with glass and stainless steel particles for the conditions in Table 2. The number of images located both at and away from the wall were obtained from photographic negatives, by using a Mitutoyo PJ311 profile projector, which is equipped with 10× to 50× zoom lens.

Figure 4 gives the results of this analysis as a plot of the effect of Reynolds number on the ratio of the number of particles located at the wall to the total number of particles in

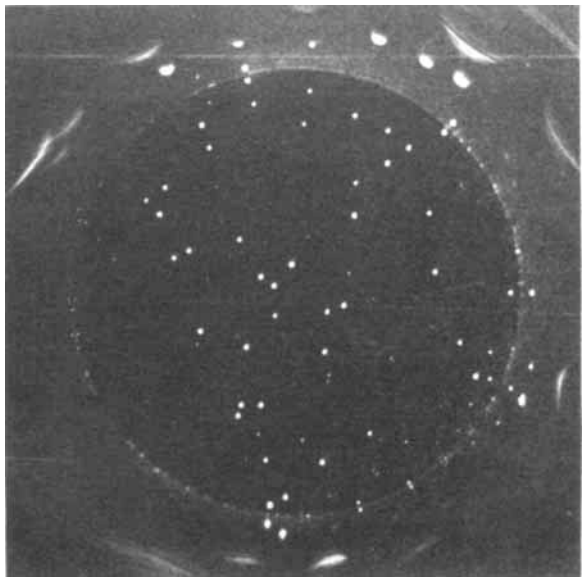

Figure 2. Single image technique of glass particles: $z = 392$ cm, $Re = 22{,}000$.

the cross-section. It should be noted that this fraction is only a measure of the tendency for trapping; it is not the same as the fraction of the total number of particles that are trapped. The figure shows that trapping of glass particles occurs for this system for Reynolds numbers less than about 26,000. At $Re = 26{,}000$, the number of glass particles trapped was so small that necklaces were not observed.

An increase in particle density was found to increase the amount of trapping. From Figure 4 it is seen that a larger Reynolds number was required to inhibit trapping for stainless steel particles than for glass particles.

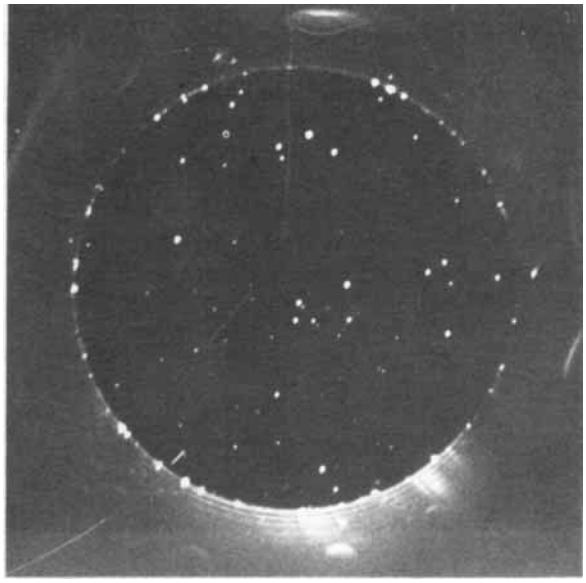

Figure 3. Single image technique of glass particles: $z = 392$ cm, $Re = 16{,}200$.

Table 2. Characteristics of Particles Used in Studies of Particle Trapping

	Re	Re_T	$d_P^+ = R^+/254$	τ^+
Glass				
$\rho_P/\rho_f = 2.42$	16,200	0.86	1.88	0.54
	18,900	0.86	2.15	0.71
	22,000	0.86	2.46	0.92
Stainless Steel				
$\rho_P/\rho_f = 8.0$	16,200	3.23	1.88	1.2
	26,100	3.23	2.85	2.8
	72,900	3.60	6.82	17.6

Concentration profiles and average velocities

Measurements of average concentration profiles and of average particle velocities in the radial direction were made by analyzing a large number of photographs obtained by axial viewing photography. Illumination of the pipe cross-section, both with single pulses and multiples pulses, was used. The conditions for these runs are in Table 3.

When particle velocities were measured, 1-cm-long cross-sections were illuminated and the particles in these illuminated cross-sections were photographed with a camera at the bottom of the pipe that viewed the flow axially upward. By sequentially illuminating the cross-section at different locations along the pipe, multiple images of particles were obtained as they moved downward. A single photograph would capture about 40 particle trajectories on average. The analysis of a number of these photographs gives statistical information about particle velocities, particle distributions, and turbulent diffusion coefficients.

Figures 5 and 6 give measurements for the glass particles at a high Reynolds number. Under these conditions, no trapping was observed. The measured concentration profile is flat and the average particle velocity in the radial direction is zero, $\overline{V}_P = 0$.

Figures 7 and 8 give concentration profiles and $\overline{V}_P$ for stainless steel particles at a low Reynolds number where a large amount of trapping was observed. The particles trapped at the wall were not considered in plotting Figure 7, so that there is actually a large increase in concentration right at the wall that is not shown. As in Figures 5 and 6, there are large variations in the measurements, because the size of the sample analyzed

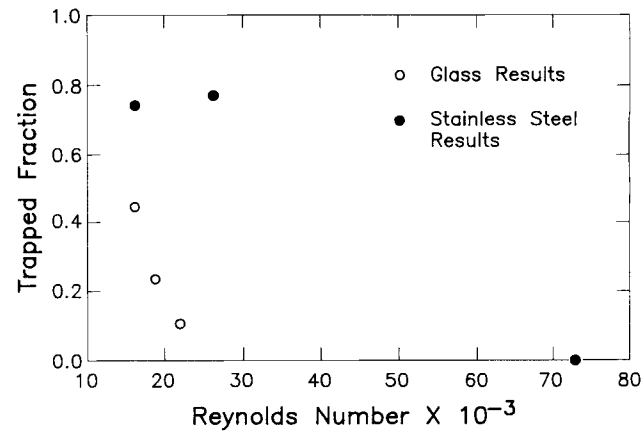

Figure 4. Trapped fraction for glass and stainless steel particles.

Table 3. Characteristics of Particles Used in Studies Particles Velocities and Concentrations

Particle	Re	$\tilde{\beta}$ (s^{-1})	U_T (cm/s)	Re_T	U_T^+	τ^+
Glass	70,800	608	0.79	0.86	0.12	7.1
Glass	16,400	604	0.79	0.88	0.46	0.54
Steel	72,900	253	3.19	3.60	0.51	17.6
Steel	15,700	265	3.05	3.23	1.77	1.2

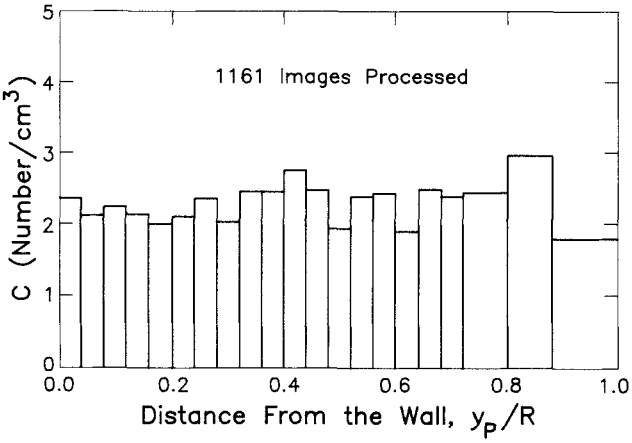

Figure 5. Particle number concentration profile for glass spheres at $Re = 70,800$.

was not large enough. However, unmistakably, the concentration is decreasing in the wall direction, and the Gaussian profile, shown in Figure 7, is a good fit to the measurements.

These results suggest that there is a net rate of trapping at the wall and that there is a diffusion of particles to the wall. This viewpoint is supported by the values of $\overline{V}_P$ in Figure 8. These may be looked on as a measure of the diffusion flux given as $\overline{V}_P\overline{C}$. If this is represented by an eddy diffusion model,

$$\overline{V}_P\overline{C} = -\epsilon_P \frac{d\overline{C}}{dr} \tag{5}$$

If ϵ_P is taken as constant then a Gaussian curve for the concentration requires that $\overline{V}_P$ increases linearly with r. This is consistent with the results shown in Figure 8, in that the flux of particles to the wall can be estimated as the product of the values of $\overline{V}_P$ and $\overline{C}$ obtained by extrapolating the Gaussian curve in Figure 7 and the straight line in Figure 8 to the wall.

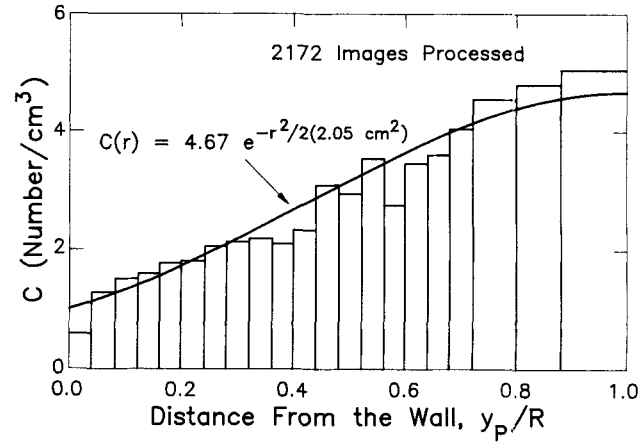

Figure 7. Particle number concentration profile for stainless steel particles at $Re = 15,700$.

The next to last bin in Figure 7 is centered at $y^+ = 30$ and the one closest to the wall at $y^+ = 10$. The sharp change in the concentration levels in these two bins could reflect a decrease in the effective turbulent diffusion coefficient, which in turn requires an increase in the concentration gradients. The flux at $y^+ < 30$ should be roughly the same as at $y^+ = 30$, so that the sharp increase in the measured $\overline{V}_P$ close to the wall, in Figure 8, is consistent with the sharp decrease in $\overline{C}$.

Interpretation

An analysis presented by Hinze (1959) suggests that the equation of motion of the particles considered in this study can be represented as:

$$\frac{dv_P}{dt} = \tilde{\beta}(v_F - v_P) \tag{6}$$

Here v_P and v_F are the radial components of the particle and

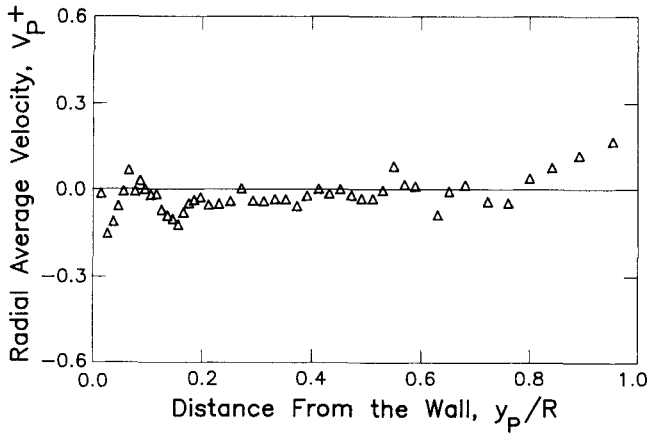

Figure 6. Radial direction average particle velocity profile for glass spheres at $Re = 70,800$.

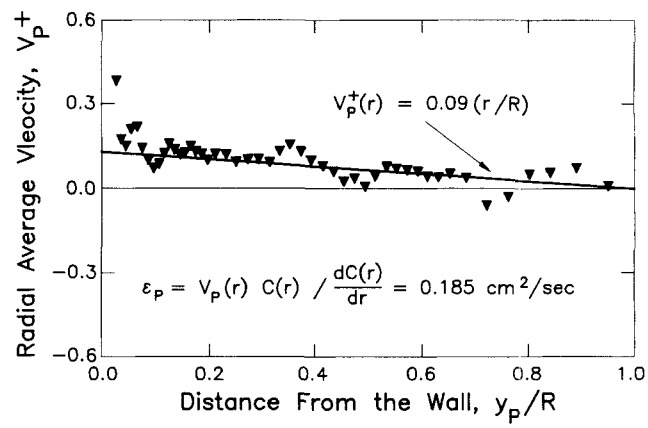

Figure 8. Radial-direction, average particle velocity profile for stainless steel particles at $Re = 15,700$.

fluid velocity fluctuations, and $\tilde{\beta}$ is a reciprocal time constant which is defined as:

$$\frac{1}{\tau^+} \equiv \tilde{\beta}^+ = \frac{3C_D}{2d_P^{+2}\left(2\frac{\rho_P}{\rho_F}+1\right)} Re_T, \tag{7}$$

when made dimensionless with wall parameters. In this equation, Re_T is a particle Reynolds number defined using d_P and U_T, the terminal velocity of a particle settling in an infinite fluid. For a Stokesian resistance, $C_D = 24/Re_T$ and Eq. 7 simplifies to:

$$\frac{1}{\tau^+} = \frac{36}{d_P^{+2}\left(2\frac{\rho_P}{\rho_F}+1\right)} \tag{8}$$

From Eq. 6 it is seen that the ability of particles to follow turbulent velocity fluctuations varies inversely with τ^+. The increased tendency toward trapping with increasing particle density (increasing τ^+) seems consistent with the notion that particles remain close to the wall because of their poor ability to respond to fluid velocity fluctuations which would move them away from the wall. However, the increasing tendency toward trapping with decreasing Reynolds number (decreasing τ^+) contradicts this interpretation. In fact, the small τ^+ associated with the experiments where trapping of glass spheres was observed suggests that these particles should be responding to turbulent velocity fluctuations close to the wall.

These considerations support the viewpoint that trapping could occur as a result of particle movement toward the wall associated with Saffman lift forces (Saffman, 1965, 1968). The derivation of Saffman predicts a time-averaged net force on particles of

$$\bar{F}_{\text{lift}} = \frac{6.46}{2}(r_P^+)\sqrt{\frac{dU_F^+}{dy^+}} Re_S \rho_F \nu^2 \tag{9}$$

if the particles are far from a boundary, if $d_P^+\sqrt{dU_F^+/dy^+}$ is a small number and if $d_P^+\sqrt{dU_F^+/dy^+} \gg Re_S$. This gives a force toward the wall if U_s is positive and a force away from the wall if U_S is negative. If the fluid resistance may be assumed to be represented by the Stokes law, this lift force can be pictured as causing a drift velocity toward the wall given by:

$$V_{\text{lift}}^+ = \frac{6.46}{12\pi}\sqrt{\frac{dU_F^+}{dy^+}} Re_S \tag{10}$$

Brenner (1961) and Maude (1961) have independently considered the steady motion of spheres toward, away from, and parallel to plane surfaces. The results for spheres moving parallel to the wall are given by Eqs. 2 and 3. For flow normal to a plane, Maude gives the drag force on a sphere as:

$$F_{D\perp} = 6C_\perp \pi \mu r_P (v_P - v_F) \tag{11}$$

$$C_\perp = \left[1 - \frac{9}{8}\frac{r_P}{y_P}\right]^{-1} \tag{12}$$

It is noted that as the ratio of the distance from the wall y_P to the particle radius r_P decreases, the lift force toward the wall will be opposed by a larger resistance than predicted by Stokes law. This would have the net effect of decreasing the drift velocity. Furthermore, this increase in fluid drag would tend to enhance the ability of the particles to follow the fluid velocity fluctuations. Equation 12 is plotted in Figure 9 as a dashed curve. Cox and Brenner (1967) have shown that Eq. 12 is not valid for very small y_P/r_P. Their calculations are shown by the points in Figure 9. The solid curve, which represents a combination of Eq. 12 and the results of Cox and Brenner, was used for our calculations.

Equation 10 can be modified in the following manner to take account of the effect of the wall on drag:

$$V_{\text{lift}}^+ = \frac{6.46}{12\pi C_\perp}\sqrt{\frac{dU_F^+}{dy^+}}\frac{Re_T}{C_{11}}, \tag{13}$$

where Re_T is defined in terms of the free-fall velocity U_T in the absence of a wall. Equation 13 is consistent with the observation of an increase in particle trapping with an increase in particle density (or Re_T). To understand the influence of fluid flow rate it is necessary to consider $C_\perp$ and C_{11}.

It is noted that $dU_F^+/dy^+ = 1$ for $y+ < 5$, that it decreases to 0.5 at $y^+ = 12$ and to 0.08 at $y^+ = 30$. Consequently, from Eq. 13, it is expected that V_{lift}^+ will become small if the particles are located much beyond $y^+ = 12$. From Eq. 13 it is noted that if $C_\perp = 1$ and $C_{11} = 1$, the drift velocity assumes its largest value at $y_P^+ < 5$. For increasing flow rate, r_P^+ increases so that at $y_P^+ = 5$ the ratio r_P/y_P increases. This has the effect of decreasing the maximum V_{lift}^+ so that an increase in liquid flow rate decreases the tendency for particle trapping.

Equation 13 is consistent with observations regarding the trapping but it does not seem to explain the location of entrapped particles at a distance of approximately one particle diameter. This is associated most likely with a lift force away from wall that results from inhibition of fluid displacement when the particle is close to the wall. This was discovered by Cox and Hsu (1977) and Vasseur and Cox (1977) in their analysis of particles sedimenting in a stationary fluid. These

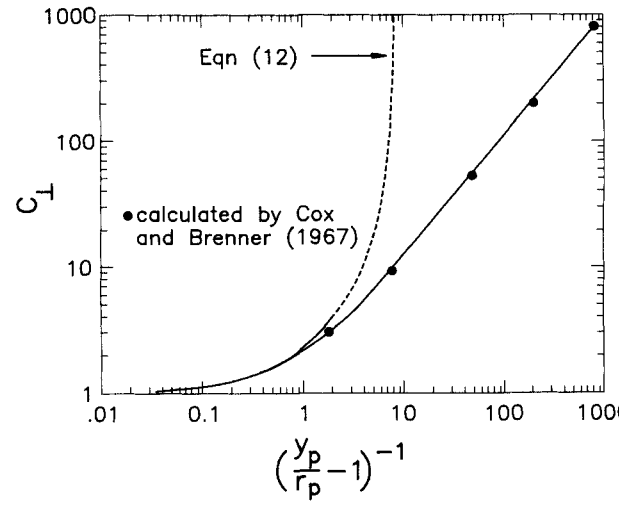

Figure 9. Correction factor for drag on particles moving perpendicular to a wall.

results have recently been confirmed experimentally by Cherukat and McLaughlin (1990). This wall-induced lift gives rise to a particle drift away from the wall at very small distances from the wall and decreases to zero for large $(y_P/d_P)Re_S$ in the following way:

$$V_{\text{wall}} = -3\nu r_P/8y_P^2, \tag{14}$$

where ν is the kinematic viscosity. As given by Vasseur and Cox (1977), this effect can be represented as:

$$V_{\text{wall}} = -\frac{3\nu r_P}{4y_P^2\pi} I\left(\frac{y_P}{d_P}Re_S\right), \tag{15}$$

where I is a tabulated function with values of $\pi/2$ and of $(\pi/8)(y_P/d_P)^2Re_S^2$ for large and small values $(y/d_P)Re_S$. Equation 14, therefore, assumes the values of

$$V_{\text{wall}} = -(3/64)Re_S U_S \tag{16}$$

at very small distances from the wall and of

$$V_{\text{wall}} = -3\nu r_P/8y_P^2 \tag{17}$$

at large distances.

The maximum value of this wall imposed drift is obtained where $dU_F^+/dy^+ = 1$ and

$$V_{\text{wall}} = -\left(\frac{3}{64}\right)\frac{Re_T U_T}{C_{11}^2} \tag{18}$$

if the effect of the wall on the terminal velocity is taken into account. By equating Eqs. 18 and 13:

$$U_T^+ = 3.66\frac{C_{11}}{C_\perp} \tag{19}$$

This defines a value of d_P/y_P at which the Saffman lift force equals the wall-imposed force.

Values of y_P/d_P calculated in this way are presented in Table 1. The value of the slip velocity U_S corrected for wall effects obtained in these calculations is $(U_T/C_{11}) = 0.43$ cm/s. The agreement is as good as could be expected, considering the accuracy of the calculation.

The value of Re_T for the data in Table 1 is 0.86. However, when corrected for the influence of the wall, a value of $Re_S = 0.47$ is obtained. Therefore, the requirement of the Saffman calculation that Re_S is small and that $d_P^+\sqrt{dU_F^+/dy^+} > Re_S$ seems to be met. However, calculated results in Table 1 give $y_P/r_P \cong 1.3$–1.8 and do not meet the requirement that $y_P \gg r_P$ in the Vasseur-Cox result on wall-induced lift. Furthermore, since the Saffman analysis is for an unbounded fluid, it is tacitly assumed in the analysis that the effect of a boundary on his result is taken into account by using the Vasseur-Cox result.

Calculations of Lift Velocities

Calculations based on the interpretation presented in the preceding section are not as accurate as would be desired because of limitations of present theories. Nevertheless, an attempt is made in this section to calculate the net drift velocity toward the wall for conditions considered in Figure 4 and Table 2.

The condition for Eq. 13 that $d_P^+\sqrt{dU_F^+/dy^+} > Re_T$ is not met if y_P^+ is too large. Therefore, a recent analysis by McLaughlin (1989) that eliminates this requirement is used. Equation 13 is thus written as:

$$V_{\text{lift}}^+ = \frac{6.46}{12\pi C_\perp}\sqrt{\frac{dU_F^+}{dy^+}}\,\frac{Re_T}{C_{11}}\,\frac{J}{2.255} \tag{20}$$

Here J is a function of the ratio $\epsilon = (d_P^+\sqrt{dU_F^+/dy^+})/(Re_T/C_{11})$ given by McLaughlin. It is equal to 2.255 for large ϵ, decreases to 1.686 for $\epsilon = 1.0$ and to 0.118 for $\epsilon = 0.3$.

From Eq. 14 the wall-induced lift could be represented as:

$$V_{\text{wall}}^+ = -\left(\frac{3}{64}\right)\frac{Re_T^2}{d_P^+ C_{11}^2}\left[\frac{8}{\pi}\frac{I(Re_l)}{Re_l^2}\right] \tag{21}$$

where $Re_l = (y_P/d_P)(Re_S)$ is a Reynolds number based on the distance of the particle from the wall and $I(Re_l)$ is the function defined in Eq. 15.

The net drift velocity toward the wall is therefore calculated as:

$$V_{\text{drift}}^+ = V_{\text{lift}}^+ + V_{\text{wall}}^+ \tag{22}$$

and is plotted in Figures 10 and 11. According to Saffman's theory the V_{drift}^+ would depend only on Re_T and $G^+ = g\nu/v^{*3}$. However, when the dependence of the drift velocity on ϵ is taken into account, an additional dependence on d_P^+ and hence, the pipe Reynolds number Re is introduced. It is noted, consistent with the discussion presented in the previous section, that the net average drift toward the wall vanishes at a finite y^+. Also plotted in Figures 10 and 11 are values of the root mean square of the turbulent velocity component normal to the wall, obtained from the thesis of Lyons (1989). Since the fluid turbulence mixes the particles, the relative importance of the drift can be determined by comparing its value with the magnitude of the turbulent velocity fluctuations.

The case for which trapping was the strongest was for experiments with stainless steel spheres at a Reynolds number of 16,200. The calculated net drift velocity is larger than the turbulence velocity for $1.2 < y_P^+ < 6.3$, and the net drift velocity is zero at $y_P^+ = 1.2$. It is noted that particles located at $y_P^+ = 1.2$ will experience a drift velocity larger than the turbulence velocity if they are displaced slightly in the direction of positive y^+ and a turbulence velocity larger than the drift if displaced in the direction of negative y_P^+. This suggests that particles located at $y_P^+ = 1.2$ will experience restoring forces if they are displaced slightly in either direction. This type of behavior is also calculated for four other conditions at which trapping was observed: stainless steel spheres at $Re = 26{,}100$; glass spheres at $Re = 16{,}200$, 18,900, and 22,000.

The calculated results for stainless steel spheres at $Re = 72{,}900$ show that vanishing of the calculated net drift velocity at $y_P^+ = 3.8$ is of no consequence, since the magnitude of the turbulent fluctuations are so large compared to the drift velocity that they will keep the particles mixed. This is consistent

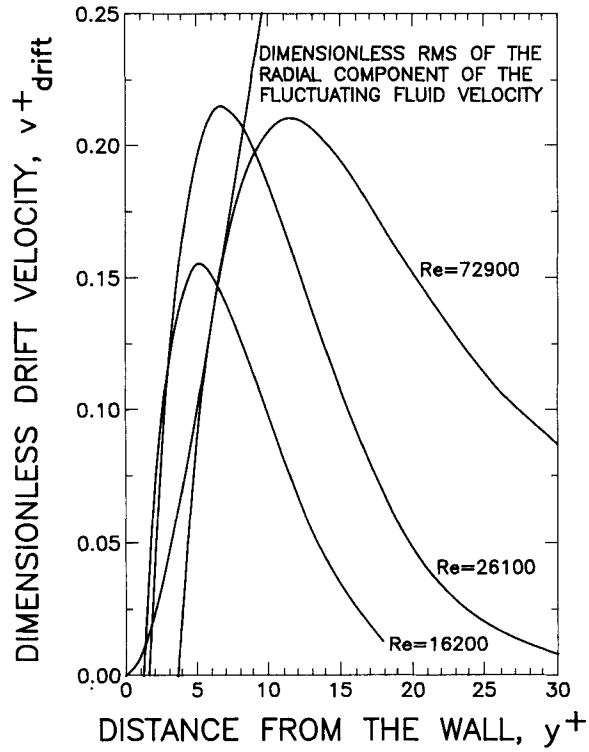

Figure 10. Calculated drift velocity toward the wall for stainless steel particles.

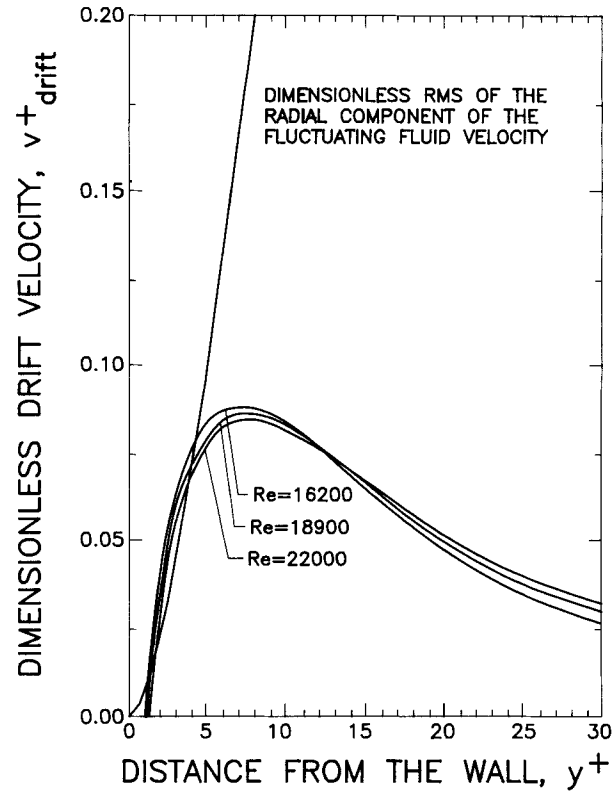

Figure 11. Calculated drift velocities toward the wall for glass particles.

with the experimental observation that there was no tendency for particles to be trapped at the wall under these conditions.

Discussion

Particles contained in a downwardly flowing turbulent fluid have been observed to be trapped, under certain conditions, in the slowly moving fluid close to the wall at a distance of about one particle diameter. The trapped particles form necklaces with spanwise spacing equal to the spacing of low-speed streaks observed close to a wall. The phenomenon has been observed to occur with extremely dilute suspensions so it cannot be associated with particle-particle interactions.

This observation can be interpreted as occurring when the drift velocity toward the wall caused by the Saffman lift force dominates the mixing associated with fluid turbulence. The experimental study of Cherukat and McLaughlin and the theoretical study of Vasseur and Cox show that when a particle is moving parallel to the wall at very small distances, the inhibition of fluid displacement by the wall causes a force on the particle away from the wall. It is argued that the particles tend to be located at a distance from the wall where the Saffman lift force is just balanced by the force due to fluid displacement.

This interpretation of the experimental results is not firmly established because of limitations of present theoretical analyses. The Saffman lift force was derived for a particle in a fluid of infinite extent, and the fluid displacement force was derived for the case of a particle sedimenting in a fluid of zero velocity. The addition of these two forces to obtain Eqs. 18 and 21 is an approximation that would not be needed if the analysis of Saffman were extended to include the effect of the wall. Furthermore, because the analysis of Vasseur and Cox assumes $Re_l > Re_S$, some numerical inaccuracy is introduced in using their result.

Acknowledgment

This work was supported by the National Science Foundation under NSF CBT 88-00980 and by the Department of Energy under DEF G02-86ER13556. The authors acknowledge the help received from George Niezyniecki with some of the calculations.

Notation

C = concentration of particles
C_D = drag coefficient
$C_\perp$ = correction on drag perpendicular to a wall due to the wall proximity
C_{11} = correction on drag parallel to a wall due to the wall proximity
d_P = particle diameter
$F_{D\perp}$ = drag force perpendicular to a wall
F_{D11} = drag force parallel to a wall
F_{lift} = Saffman lift force
I = function in Eq. 14 associated with wall-induced lift
J = function in Eq. 16 associated with McLaughlin correction to Saffman lift force
r = radial coordinate
R = pipe radius
r_P = particle radius
Re = Reynolds number based on pipe diameter and bulk fluid velocity
Re_l = Reynolds number based on slip velocity and distance of a particle from the wall
Re_S = Reynolds number based on slip velocity and particle diameter
Re_T = Reynolds number based on terminal velocity and particle diameter
t = time
u^* = friction velocity

U_P = mean particle velocity in the mean flow direction
U_T = terminal velocity of a particle in stationary fluid
U_F = mean fluid velocity in the axial direction
U_S = mean slip velocity of particle
V_P = mean particle velocity in the radial direction
V_{lift} = drift velocity toward the wall caused by Saffman lift force
V_{wall} = drift velocity toward the wall associated with wall-induced force
v_P = fluctuating particle velocity in the radial direction
v_F = fluctuating fluid velocity in the radial direction
y = distance from the wall
y_P = distance of the center of a particle from the wall

Greek letters

$\tilde{\beta}$ = coefficient appearing in the particle equation of motion
ϵ = $((dU_F/dy)\nu)^{1/2}/U_S$
ϵ_P = particle diffusion coefficient
μ = fluid dynamic viscosity
ν = fluid kinematic viscosity
ρ_F = fluid density
ρ_P = particle density
τ = particle time constant equal to $\tilde{\beta}^{-1}$

Superscript

$+$ = made dimensionless using friction velocity and fluid kinematic viscosity

Literature Cited

Brenner, H., "Slow Motion of a Sphere Through Viscous Fluid Toward Plane Surface," *Chem. Eng. Sci.*, **16**, 242 (1961).

Cherukat, P., and J. B. McLaughlin, "Wall-Induced Lift on a Sphere," *Int. J. Multiphase Flow*, **16**, 899 (1990).

Cox, R. G., and H. B. Brenner, "The Slow Motion of a Sphere Through a Viscous Fluid Towards a Plane Surface II. Small Gap Widths, Including Inertial Effects," *Chem. Eng. Sci.*, **22**, 1753 (1967).

Cox, R. G., and S. K. Hsu, "The Lateral Migration of Solid Particles in a Laminar Flow Near a Plane," *Int. J. Multiphase Flow*, **3**, 201 (1977).

Goldman, A. J., R. G. Cox, and H. B. Brenner, "Slow Viscous Motion of a Sphere Parallel to a Plane Wall: II. Couette Flow," *Chem. Eng. Sci.*, **22**, 653 (1967).

Hinze, J. O., *Turbulence*, McGraw Hill, New York (1955).

Lyons, S. L., "A Direct Numerical Simulation of Fully Developed Channel Flow with Passive Heat Transfer," PhD Thesis, Univ. of Illinois, Urbana (1989).

Maude, A. D., "End Effects in a Falling Film Viscometer," *Brit. J. Appl. Phys.*, **12**, 293 (1961).

McLaughlin, J. B., "Inertial Migration of a Small Sphere in Linear Shear Flows," *J. of Fluid Mech.*, **224**, 261 (1991).

Saffman, P. G., "The Lift on a Small Sphere in a Slow Shear," *J. Fluid Mech.*, **22**, 385 (1965).

Saffman, P. G., "Corrigendum to the Lift on a Small Sphere in a Slow Shear Flow," *J. Fluid Mech.*, **31**, 624 (1968).

Segre, G., and A. Silberberg, "Behavior of Microscopic Rigid Spheres Poiseuille Flow," *J. Fluid Mech.*, **14**, 115 (1962).

Vasseur, P., and R. G. Cox, "On the Motion of a Small Spheroidal Particle in a Viscous Liquid," *Int. J. Multiphase Flow*, **3**, 201 (1977).

Young, J. B., "An Experimental Study of Solid Particle Motion in a Turbulent Liquid Pipe Flow," PhD Thesis, Univ. of Illinois, Urbana (1989).

Manuscript received Jan. 4, 1991, and revision received Aug. 16, 1991.